TISSUE ENGINEERING: Part A
Volume 20, Numbers 23 and 24, 2014

DOI: 10.1089/ten.tea.2013.0753

Architectural and Mechanical Cues Direct Mesenchymal Stem Cell Interactions with Crosslinked Gelatin Scaffolds

Kathleen M. McAndrews, BS,[1] Min Jeong Kim, BS,[1] Tuyet Y. Lam, BS,[2]
Daniel J. McGrail, BS,[1] and Michelle R. Dawson, PhD[1,3]

Naturally derived biomaterials have emerged as modulators of cell function and tissue substitutes. Here, we developed crosslinked glutaraldehyde (GTA) scaffolds for the expansion and differentiation of mesenchymal stem cells (MSCs). The mechanical and architectural properties of the scaffolds were altered by varying the concentration of gelatin and GTA. Higher GTA concentrations were associated with an increase in more confined pores and osteogenic differentiation. In addition, myogenic potential varied with crosslinking degree, although bulk mechanical properties were unaltered. Correlation analysis revealed that ALP activity of differentiated MSCs on higher gelatin concentration scaffolds was dependent on traditional effectors, including environment elasticity and spread area. In contrast, the differentiation capacity of cells cultured on lower gelatin concentration scaffolds did not correlate with these factors, instead it was dependent on the hydrated pore structure. These results suggest that scaffold composition can determine what factors direct differentiation and may have critical implications for biomaterial design.

Introduction

The ability to transplant organs and tissues has saved many lives and revolutionized the field of medicine; however, limitations in available donor organs and tissues, high costs associated with transport surgeries, and poor compliance with lifetime regimens of immunosuppressive drugs reduce the number of patients who can benefit from this therapy. Tissue engineering provides an alternative source to obtain tissues and organs that can be used to replace or regenerate tissues damaged by disease, congenital abnormalities, or traumatic injury. Naturally derived polymers, including collagen and gelatin, have been proposed as potential tissue substitutes because they are nonimmunogenic, biocompatible, and biodegradable. Gelatin, which is denatured collagen, is a relatively inexpensive, FDA-approved biomaterial that has been utilized in a variety of applications[1–3]; however, its applicability in the clinic is limited by its poor mechanical strength. Glutaraldehyde (GTA) has been used as a crosslinker to enhance the mechanical properties of collagen-based scaffolds[4] because of its low cost and ease of availability. In addition, GTA has been used clinically in prosthetic implants. Although GTA can be toxic to cells, it can be neutralized by glycine.[5]

The addition of cells to a regenerative biomaterial can further enhance the healing process. Mesenchymal stem cells (MSCs) are multipotent adult bone marrow-derived stem cells that can differentiate into various connective tissues, including bone, fat, and cartilage.[6] MSCs have shown promise for tissue regeneration applications because they are easily accessible, are immunosuppressive,[7] and do not undergo tumorigenesis *in vivo*[8] and have been used for a variety of applications clinically, including liver disease,[9] subcutaneous wounds,[10] and osteogenesis imperfecta.[11] The implementation of MSCs in the clinic has been limited by low implanted cell survival rates[12] and an incomplete understanding of how MSC differentiation is affected by the microenvironment.[13] Biomaterials can affect cell proliferation, differentiation, extracellular matrix secretion and remodeling, and formation of functional tissues; thus, they have shown promise for directing cell function[14] and MSC differentiation.[15–17] Numerous studies have highlighted the effects of physical and chemical cues from the tissue microenvironment on MSC differentiation,[17–20] though the role of the three-dimensional architecture has not been fully elucidated. We hypothesized that it was not just the bulk mechanical properties of tissue-engineered scaffolds but the microscopic architecture of these environments that direct MSC fate.

[1]School of Chemical and Biomolecular Engineering, Georgia Institute of Technology, Atlanta, Georgia.
[2]School of Chemistry and Biochemistry, Georgia Institute of Technology, Atlanta, Georgia.
[3]The Petit Institute for Bioengineering and Bioscience, Georgia Institute of Technology, Atlanta, Georgia.

In these studies, we fabricated gelatin-GTA scaffolds and altered the mechanical properties (bulk elastic moduli of ~10–40 kPa) and architectural properties (pore size and fiber structure) by varying the concentration of gelatin and GTA. Osteogenic differentiation was induced on scaffolds with relatively low amounts of GTA (0.1–1.0% w/v). In addition, myogenic potential varied on scaffolds with similar bulk mechanical properties. We found that mechanical properties of the scaffold and the extent of cell spreading directly correlated with osteogenic differentiation on 10% (w/v) gelatin scaffolds, whereas on 5% gelatin scaffolds, the hydrated microscale pore structure played a stronger role in directing differentiation. These results suggest that in addition to matrix stiffness, cells also sense architectural properties of their local environment and integrate these cues when undergoing lineage commitment. By elucidating the interplay of these two factors, this work seeks to improve matrix-directed MSC differentiation.

Materials and Methods

Materials

Gelatin was purchased from Sigma Aldrich. Iscove's Modified Dulbecco's Medium (IMDM), L-glutamine, and penicillin-streptomycin were purchased from Corning. Premium select fetal bovine serum (FBS) was purchased from Atlanta Biologicals (Lot L12163). Fluorosphere-carboxylate-modified 200-nm red particles were purchased from Invitrogen. All other materials were purchased from VWR.

Preparation of scaffolds

Gelatin (G) was dissolved in distilled water for 15 min at 70°C under magnetic stirring to make 5 and 10 wt% solutions. A 5% GTA solution was then added to mixtures to form 0.1, 0.5, and 1.0 wt% solutions. The mixture was vortexed and then cast. The scaffolds were refrigerated at 4°C before use. Scaffolds were lyophilized for scanning electron microscopy (SEM) imaging and water-absorption studies.

Mechanical testing

Gelatin scaffolds were prepared in a petri dish. After 24 h, scaffolds were cut into three sections and rehydrated in phosphate-buffered saline (PBS). The Young's modulus was measured by compression testing using a Bose Endura TEC ELF 3200 Uniaxial Testing System. The Young's modulus was calculated from the slope of the stress-versus-strain curve in the linear region at $<10\%$ strain using the following equation:

$$E = \frac{FL_0}{A_0 \Delta L}$$

F is force exerted, A_0 is initial area of the scaffold, ΔL is change in length, and L_0 is initial length.

SEM imaging

Lyophilized scaffolds were coated with gold for 30 s using gold sputter coater. Scaffolds were imaged using a Hitachi S800 field emission gun scanning electron microscope. The pore area was calculated by manually tracing the pores in ImageJ software (NIH). To calculate surface area, gelatin fibers were segmented in a custom-written MATLAB algorithm after convolution with a LaPlacian of Gaussian (LoG) mask.

Multiple-particle tracking microrheology

Twenty-second videos of the thermal displacements of 200-nm carboxylated particles embedded in the scaffold were captured using a Photometrics QuantEM CCD camera at 30 frames per second and a Nikon epifluorescent microscope with a TIRF 100× lens (Nikon) at 37°C. The coordinates of the particles were determined and analyzed using a custom-written MATLAB algorithm. Briefly, a bandpass filter was applied to the images and the centroid of the particle was determined with subpixel accuracy as described previously.[21] Particle trajectories were determined using a Hungarian linker algorithm. The mean square displacements (MSDs) were calculated using a previously described custom MATLAB algorithm[22,23] and the following equation: $<\mathrm{MSD}(\tau)> = <[x(t+\tau) - x(t)]^2 + [y(t+\tau) - y(t)]^2>$. MSD can be described by a power law: $<\mathrm{MSD}(\tau)> = 4D\tau^{\alpha}$, where D is the diffusion coefficient and α is the anomalous diffusion coefficient. The anomalous diffusion coefficient can be used to describe the motion of the particle, with $\alpha = 0$ characteristic of a Hookean solid, $\alpha = 1$ characteristic of a Newtonian fluid, and $0 < \alpha < 1$ characteristic of a viscoelastic fluid. The slope of the logarithmic MSD curve (α) was calculated by using finite difference between $\tau = 1$ s and $\tau = 10$ s. Any slope greater than one (indicative of convective transport) or less than zero was automatically excluded from analysis to eliminate the effects of motion artifact from sample drift.

Water-absorption test

Lyophilized scaffolds were weighed to obtain dry weight (W_d). Cell culture growth media were added to the scaffold to reach saturation. Samples were incubated at 37°C to mimic culture conditions. The wet weight (W_w) of each scaffold was obtained after 24, 48, 72, and 96 h. The water-absorption ability of the scaffolds was calculated with the following equation:

$$\textit{Media absorption}(\textit{n-fold}) = \frac{W_w - W_d}{W_d}$$

Degradation

PBS solution was added into polymerized scaffolds and incubated at 37°C. The supernatant was collected at 24, 48, and 72 h. Bicinchoninic acid assay was used to determine the amount of gelatin released using a standard curve.

Cell culture

MSCs were isolated from 4-week-old Balb/C mice (Jackson Laboratory) as described previously.[22] Cells were cultured in IMDM supplemented with 20% FBS, 2 mM L-glutamine, and 100 U/mL penicillin-streptomycin. Flow cytometry was performed to confirm that cells were Sca-1$^+$, CD29$^+$, CD105$^+$, CD11b$^-$, and CD45$^-$, and osteogenic and adipogenic assays on tissue culture plastic were performed to confirm the MSC phenotype (data not shown). For

all experiments, gelatin was autoclaved prior to scaffold formation. Uncrosslinked GTA was neutralized by multiple changes of 1% glycine, and 10 μg/mL of human fibronectin was added to promote cell adhesion.

Cell proliferation

MSCs were seeded on scaffolds at a density of 5000 cells per scaffold (10,000 cells/cm^2) in order to allow space for proliferation and cultured for 3 days. The cells were then removed by trypsinization, resuspended in Isoton II solution, and counted using a Beckman Coulter Multisizer 3 Coulter Counter. Proliferation index was calculated as the number of cells for each condition divided by the overall average number of cells for each experiment.

MSC differentiation

For osteogenesis experiments, MSCs were cultured on scaffolds in either control media (IMDM, 20% FBS, 1% penicillin-streptomycin, and 1% L-glutamine) or osteogenic media (IMDM, 20% FBS, 1% penicillin-streptomycin, 1% L-glutamine, 10 nM dexamethasone, 20 nM β-glycerolphosphate, 50 μM ascorbate-2-phosphate, and 50 ng/mL L-thyroxine sodium pentahydrate) as described previously[24] for 3 weeks. Cells were then fixed with formalin and stained for ALP expression using NBT/BCIP reagent. Images were taken using a Nikon SMZ745T stereoscope. ALP activity was determined from the absorbance at 595 nm of cells cultured in osteogenic media normalized by absorbance of cells cultured in control media. For myogenic differentiation, MSCs were cultured on scaffolds in control media supplemented with 10 ng/mL human recombinant TGF-β1 (Biolegend) for 1 week.

Gene expression analysis

RNA was isolated from MSCs cultured on scaffolds in osteogenic media for 3 weeks or myogenic media for 1 week using Ribozol reagent (Amresco) and reverse transcribed to cDNA using iScript cDNA synthesis kit (BioRad). Gene expression analysis was not performed on cells cultured on 10% gelatin–0.1% GTA scaffolds due to low cell numbers. Primers were designed using Primer3 software.[25] Quantitative real-time polymerase chain reaction was performed on the target sequences listed in Table 1 using SsoAdvanced SYBR Green Mastermix (BioRad) in a StepOne Plus Thermocycler (Applied Biosystems) for 40 cycles. For osteogenesis experiments, data were reported after normalization to endogenous *GAPDH* and expression of cells cultured on 5% gelatin–0.1% GTA scaffold. Data for myogenesis were normalized to *GAPDH* and Wilcoxon-Mann-Whitney rank sum test was used for statistical analysis.

Statistical analysis

All experiments were performed in triplicate. Unless otherwise noted, a Student's *t*-test was used for statistical analysis with $p < 0.05$ being statistically significant ($*p < 0.05$, $**p < 0.01$, and $***p < 0.001$) and data were reported as the mean ± standard error of the mean.

Results

Characterization of gelatin-GTA scaffolds

The Young's moduli of 5% (w/v) gelatin (G) scaffolds were relatively constant (~15 kPa) across GTA concentrations (Fig. 1A). The bulk mechanical properties of 10% G–0.1% (w/v) GTA scaffolds were similar to 5% scaffolds. Higher concentrations of GTA were associated with approximately threefold increase in bulk stiffness for 10% scaffolds (~50 kPa). To determine the stability of the scaffolds, we measured protein release over time. Scaffolds with 0.1% GTA released more gelatin than those containing 0.5% and 1% GTA ($p < 0.05$); however, low amounts of protein were released from all scaffolds, suggesting that they remain intact (Fig. 1B). All scaffolds swelled ~7- to 15-fold within 1 day and then remained relatively constant over a 7-day period (Fig. 1C). Swelling in 5% gels was relatively independent of GTA concentration, while in 10% gels, swelling was significantly reduced in 0.5% and 1% GTA concentrations compared with 0.1% GTA ($p < 0.01$). Together these data suggest that the scaffolds are relatively stable for tissue engineering applications.

Scaffold composition alters pore architecture

To analyze the architecture of the scaffolds, we imaged the scaffolds using SEM and quantified pore size. Average

Table 1. Primers Used for Quantitative Real-Time Polymerase Chain Reaction

Gene	*Primer sequence*	*Accession number*
GAPDH	Forward: 5′-AGGTCGGTGTGAACGGATTTG Reverse: 5′-TGTAGACCATGTAGTTGAGGTCA	NM 008084
ALP	Forward: 5′-TCAGGATGAGACTCCCAGGA Reverse: 5′-GTGTGTGTGTGTGTCCTGTC	NM 007431
Osteocalcin	Forward: 5′-CAGTATGGCTTGAAGACCGC Reverse: 5′-AGAGAGAGAGGACAGGGAGG	NM 007541
Osteopontin	Forward: 5′-GAGAGCGAGGATTCTGTGGA Reverse: 5′-CGACTGTAGGGACGATTGGA	NM 001204201
Myogenin	Forward: 5′-ACCTTCCTGTCCACCTTCAG Reverse: 5′-CACCGACACAGACTTCCTCT	NM 031189
MyoD	Forward: 5′-TGGTTCTTCACGCCCAAAAG Reverse: 5′-ACTTCTGCTCTTCCCTTCCC	NM 010866

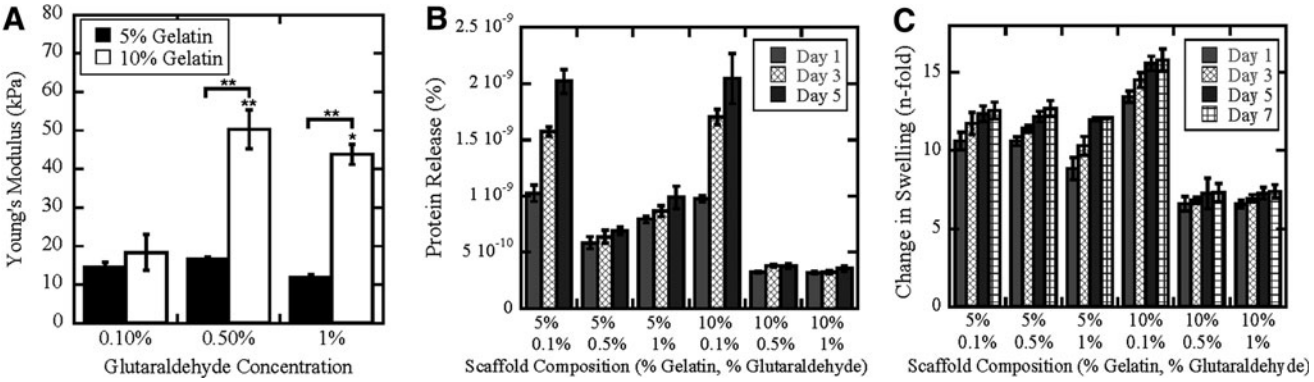

FIG. 1. Characterization of gelatin-glutaraldehyde scaffolds. The effect of scaffold composition on the mechanical properties **(A)** and degradation **(B)** and swelling **(C)** characteristics was determined. * and ** denote $p<0.05$ and $p<0.01$, respectively.

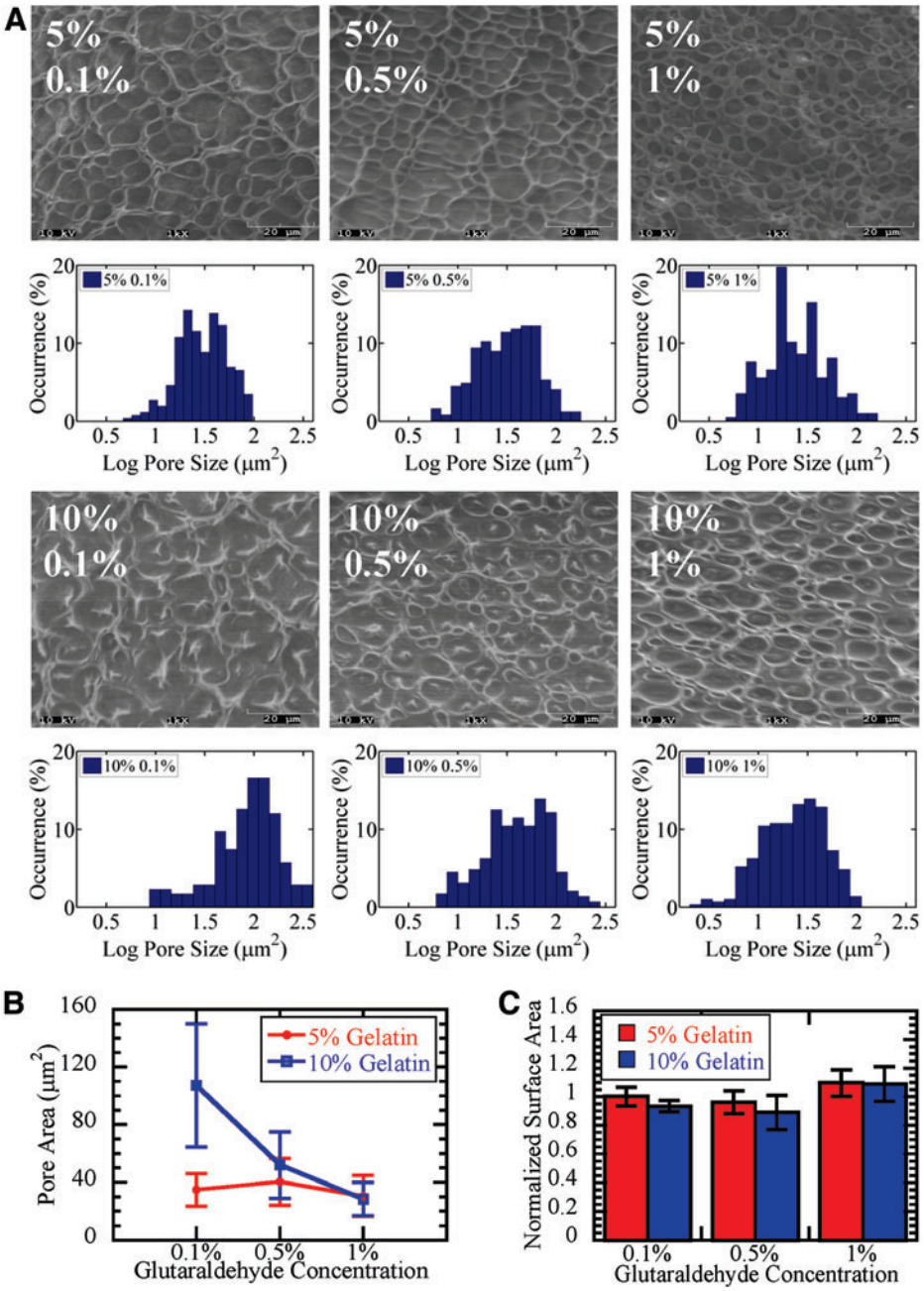

FIG. 2. Effect of scaffold composition on pore architecture. Pore sizes were quantified from scanning electron microscopy images **(A)**. Pore size was relatively constant across glutaraldehyde concentrations for 5% gelatin scaffolds and decreased for 10% gelatin scaffolds **(B)**. Surface area available for cell attachment was approximately constant across scaffold compositions **(C)**. Color images available online at www.liebertpub.com/tea

pore size was similar for 5% G–0.1% GTA and 5% G–0.5% GTA scaffolds (30–40 μm^2). The 10% G–0.1% GTA scaffold had the largest average pore size (100 μm^2). In addition, 10% G scaffolds had larger fibers than 5% G scaffolds. The highest GTA concentration was associated with a smaller pore size. For 1% GTA concentrations, average pore size was independent of gelatin concentration; however, the variation was higher in 10% scaffolds, suggesting a more heterogeneous distribution of pore sizes (Fig. 2A, B). Although the pore size distribution varied with scaffold composition, the surface area available for cell attachment was relatively constant (Fig. 2C).

Increasing GTA concentration leads to more confined pores

We utilized multiple-particle tracking microrheology (MPTM) to probe the pore structure of hydrated scaffolds in cell-culture-relevant conditions. The embedded particles underwent thermal Brownian motion that was evaluated by tracking the *x-y* coordinates of the particles. Unlike SEM that has a characteristic length scale of several microns, MPTM has a characteristic length scale of $\sim$100 nm. The extent of motion can be determined by calculating the MSD. MSD is time dependent for viscous fluids and time independent for elastic solids. MSD plots revealed that all scaffolds behaved as elastic solids at short-time scales and viscous fluids at long-time scales (Fig. 3A). Particle MSDs in scaffolds containing 0.1% GTA compared with higher amounts of GTA had decreased magnitude and increased heterogeneity in particle MSDs at $\tau = 1$ s (Fig. 3B). This suggests that a distribution of particle motions exists, with a portion of particles that displayed increased motion, whereas others did not, indicating that these particles were likely confined by the microstructure of the hydrated scaffold. In addition, particles in scaffolds with higher concentrations of GTA displayed a decreased average slope (anomalous diffusion coefficient, α) at long-time scales than those with 0.1% GTA. Because α can be used to describe the relative viscoelastic character of the fluid surrounding particle, with $\alpha = 0$ characteristic of a Hookean elastic solid, $\alpha = 1$ characteristic of a Newtonian viscous fluid, and $0 < \alpha < 1$ characteristic of a viscoelastic fluid, we further analyzed individual particles to determine whether the particles are more confined ($\alpha < 0.5$) or less confined ($\alpha > 0.5$) by the pore structure. All scaffolds had a characteristic relaxation time at approximately $\tau = 1$ s; therefore, we analyzed α from $\tau = 1$ s to $\tau = 10$ s. The percentage of less-confined particles was similar for 0.1% and 0.5% GTA concentrations independent of gelatin concentration. Crosslinking with 1% GTA was associated with a significant decrease in particles that were less confined, suggesting that there is a higher percentage of smaller pores in this condition (Fig. 3C).

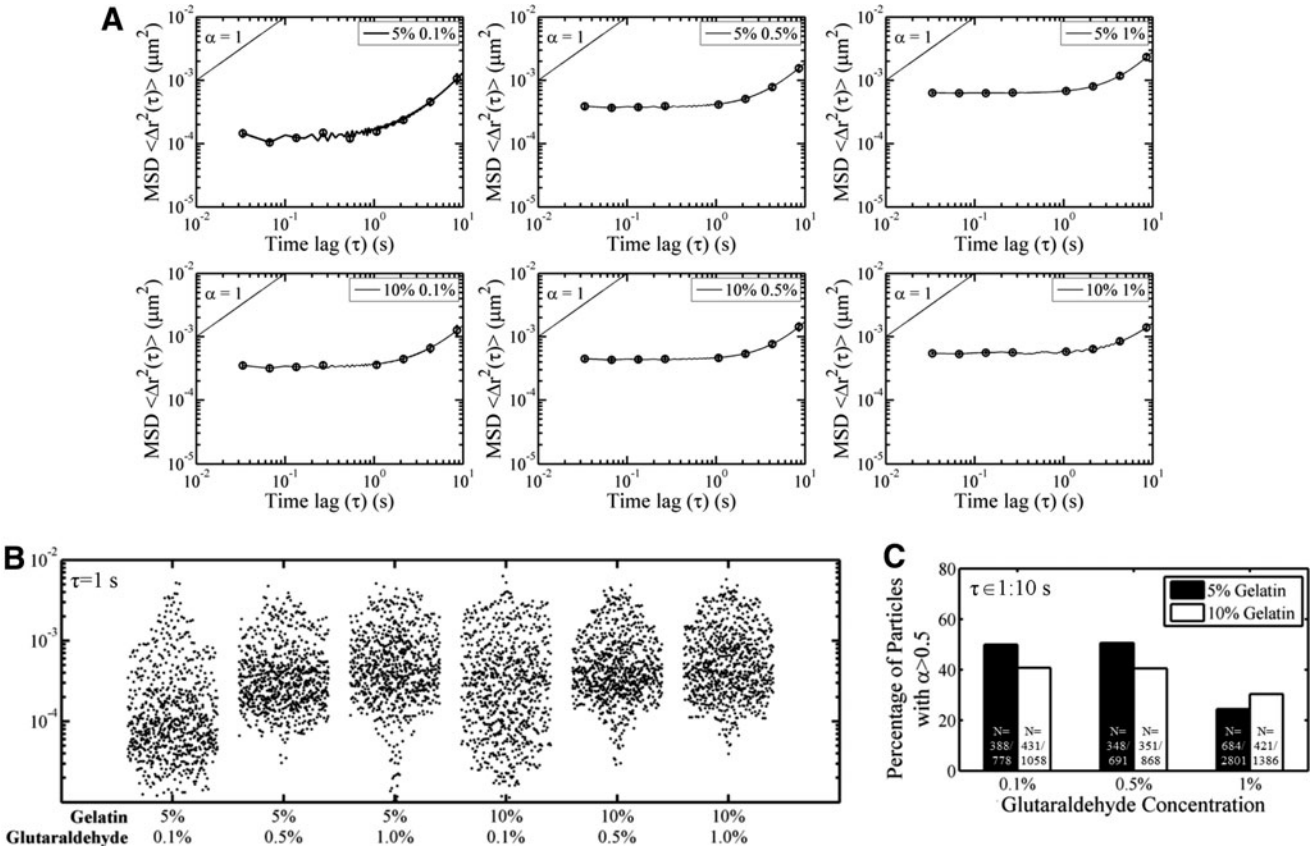

FIG. 3. Variation in mean square displacement (MSD) and confinement of particles with changes in scaffold composition. Average particle MSDs **(A)**, dot plot of individual particle MSDs at $\tau = 1$ s **(B)**, and the percentage of less-confined particles with $\alpha > 0.5$ between $\tau = 1$ s and $\tau = 10$ s **(C)** were determined under cell culture conditions.

Scaffold composition affects proliferation and differentiation potential

To determine the effect of scaffold composition on cellular function, we performed spreading, proliferation, and differentiation assays. After 24 h on the scaffolds, images of the cells were taken (Fig. 4A). Although cell spreading increased with GTA concentration, the amount of gelatin did not significantly affect cell spreading (Fig. 4B). At day 3 on the 5% G, there were significantly more MSCs on the 0.5% GTA and 1% GTA scaffolds than on the 0.1% GTA scaffold (Fig. 4C). A similar trend was found by measuring MTT absorbance, with similar viability for cells on 5% G scaffolds (Fig. 4D). Viability was significantly decreased on the 10% G–0.1% GTA scaffold. In addition, cells cultured on 5% G–1% GTA scaffolds were significantly more viable than cells on 10% G–1% GTA scaffolds.

We next sought to determine how the mechanical and architectural properties of the scaffolds affected differentiation potential. Because MSCs have increased differentiation potential along the myogenic and osteogenic lineages on two-dimensional (2D) substrates with elasticities similar to the scaffolds we developed,[19] we performed both osteogenic and myogenic induction on gelatin scaffolds. Cells were differentiated along the osteogenic lineage on scaffolds for 3 weeks and stained for ALP activity (Fig. 5A). Osteogenic differentiation was inhibited on the 10% G–0.1% GTA scaffold. Although 5% G scaffolds displayed similar mechanical properties, osteogenic potential varied with GTA concentration (Fig. 5B). Gross imaging of the scaffolds after 3 weeks of differentiation revealed enhanced mineralization in the 5% G (Supplementary Fig. S1; Supplementary Data are available online at www.liebertpub.com/tea), in agreement with ALP activity results. Gene expression of osteopontin and osteocalcin was increased in cells cultured on 5% G scaffolds with increasing GTA concentrations (Fig. 5C). In addition, cells differentiated on the 10% G–1% GTA scaffold had significantly less ALP activity and lower expression of osteocalcin, and consequently less differentiation, than the 5% G–1% GTA scaffold. To evaluate whether gelatin scaffolds enhance differentiation along other lineages, cells were differentiated in myogenic media. Myogenin and *MyoD* were upregulated in cells cultured on 5% G–1% GTA scaffolds compared with 10% G–1% GTA scaffolds (Fig. 5D). Similar to osteogenic differentiation results, myogenic potential varied with GTA concentration for 5% G scaffolds.

Discussion

In this study, we developed gelatin scaffolds with differing mechanical properties and pore sizes by altering the concentrations of gelatin and GTA. Glycine was used in these studies to neutralize GTA and circumvent GTA toxicity issues. Typically hydrated gelatin scaffolds have extremely low mechanical strength[3] and high swelling and degradability,[26] limiting their use as biomaterials; however, gelatin scaffolds crosslinked with GTA displayed enhanced mechanical properties and stability (Fig. 1). Notably, increasing GTA from 0.1% to 0.5% resulted in a twofold decrease in degradation (Fig. 1B). SEM images of 10% G–0.1% GTA scaffolds showed that the gelatin was not completely crosslinked (Fig. 2), which may be why this scaffold had a lower elasticity and higher swelling (Fig. 1).

Although bulk mechanical properties were not dependent on GTA concentration for 5% G scaffolds (Fig. 1A), pore architecture changed with additional GTA (Fig. 2). At

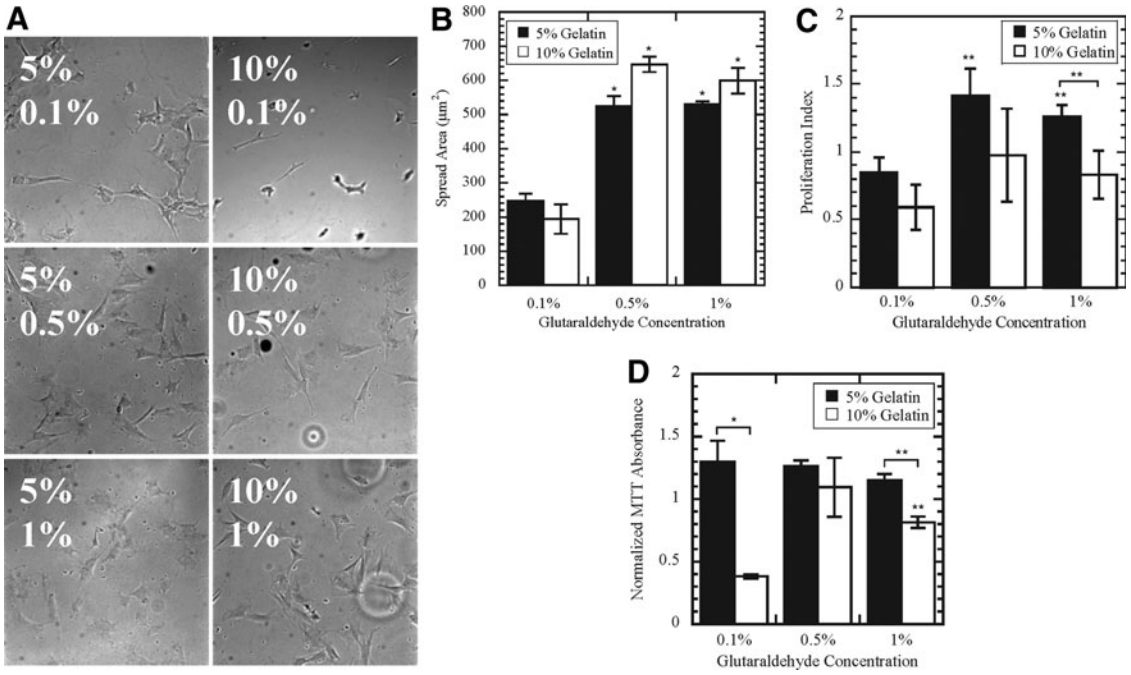

FIG. 4. Changes in mesenchymal stem cell (MSC) spreading and proliferation on scaffolds. The spreading of MSCs on the scaffold was quantified **(B)** based on phase-contrast images **(A)**. Scaffold composition altered the proliferation and viability of MSCs cultured on the scaffolds for 3 days, as measured by cell count **(C)** and MTT absorbance **(D)**. * and ** denote $p < 0.05$ and $p < 0.01$, respectively.

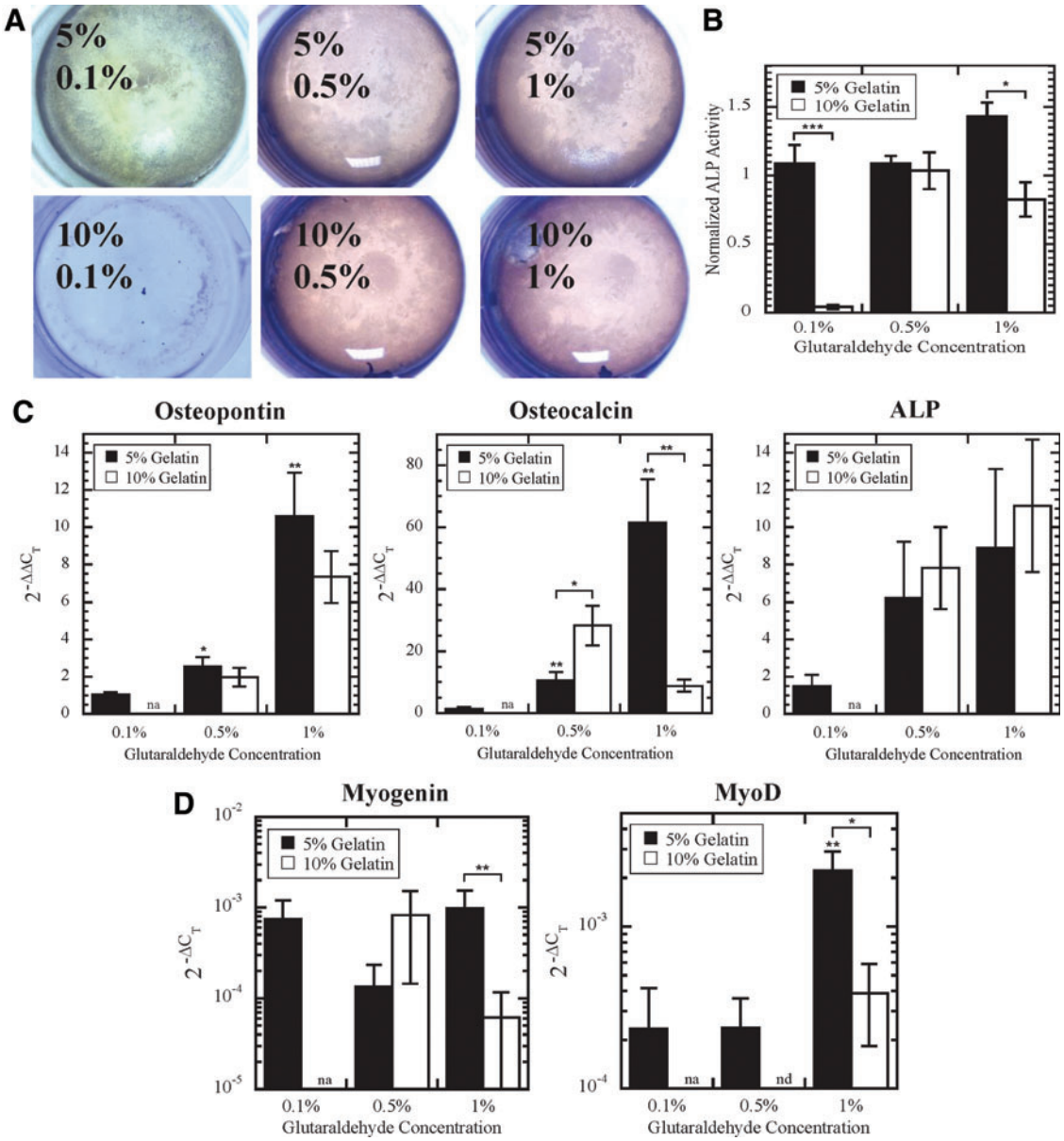

FIG. 5. Differentiation capacity of MSCs cultured on scaffolds. Osteogenic differentiation capacity of MSCs was determined by staining for ALP activity **(A)** and quantified by absorbance at 595 nm **(B)**. Expression of genes associated with osteogenic **(C)** and myogenic differentiation **(D)**. na, gene expression analysis not performed due to low cell numbers; nd, no detection of gene of interest. *, **, and *** denote $p < 0.05$, $p < 0.01$, and $p < 0.001$, respectively. Color images available online at www.liebertpub.com/tea

the two higher GTA concentrations, the average pore sizes were similar for 5% G and 10% G gels; however, the standard deviations of the pore size distributions were different (Fig. 2). These data suggest that measuring bulk or average properties alone may not accurately capture the properties of the material. In addition, samples were lyophilized for analysis that may not be representative of culture conditions. To analyze the pore structure while the scaffold is in cell culture conditions, we utilized MPTM. While SEM can probe pore structure on the order of several microns, MPTM probes a much smaller length scale, ~100 nm. All scaffolds behaved like elastic solids at short-time scales and viscoelastic fluids at longer time scales (Fig. 3A). In addition, particles encountered a heterogeneous microenvironment, consistent with MPTM results in other polymers.[27] The magnitude of the average MSD was similar for all 10% G scaffolds, but 5% G show an increasing magnitude with increasing GTA (Fig. 3A). This may be a result of polymerization kinetics as increased crosslinker concentration[28] and polymer concentration[29] have been associated with increased polymerization rates. High amounts of polymer may lead to rapid polymerization, causing the formation of a network of heterogeneous fiber sizes. For lower amounts of polymer, more crosslinker is available, leading to the formation of more uniform smaller fibers (Fig. 2A, 5% G–1% GTA). Larger fibers were seen in the SEM images of scaffolds formulated with low GTA concentrations (Fig. 2A, 10% G–0.1%

GTA). These partially crosslinked scaffolds were also less stable (Fig. 1B, C), so smaller fibers may have been destroyed during lyophilization. For these low-GTA scaffolds, particle-tracking results revealed a population of particles with more restricted transport at small time scales (Fig. 3B). This suggests that these smaller fibers present in the hydrated gels reside in fluid-filled pores where they restrict particle transport. This restricted transport is not seen at higher time scales when the gels have sufficient time to relax. In this case, a larger percentage of particles in 1% GTA scaffolds were more confined (Fig. 3C).

Though previous studies have shown that MSCs proliferate more in stiffer environments,[30] our results suggest that stiffness alone is not predicative of MSC proliferation on gelatin-GTA scaffolds (Fig. 4C, D). In addition, matrix elasticity can direct MSC lineage toward cell types with similar elasticity *in vivo*.[19] MSC myogenic potential has been enhanced on 2D substrates with elasticities around 10 kPa,[19,31] similar to the elasticity of 5% G scaffolds. While myogenin expression was relatively constant across GTA concentrations for 5% G scaffolds, *MyoD* was significantly upregulated on 5% G–1% GTA scaffolds (Fig. 5D), suggesting that the bulk mechanical properties alone do not direct MSC myogenic differentiation on gelatin scaffolds.

Numerous studies have also shown that MSCs have increased propensity to differentiate into osteoblasts in stiffer environments.[19,32] MSCs differentiated on 5% G–1% GTA scaffolds had enhanced expression of osteopontin and osteocalcin (Fig. 5C), which are late-stage osteogenesis markers, suggesting that this scaffold composition not only enhanced differentiation, but also generated a more terminally differentiated cell. Interestingly, on the scaffolds, MSCs did not display enhanced differentiation on 10% G scaffolds, which had higher elastic moduli. Young's modulus correlated with ALP activity for 10% G scaffolds ($R^2 = 0.99$, Fig. 6A). Pore size and osteogenic differentiation potential were weakly inversely correlated for both 5% G ($R^2 = 0.70$) and 10% G scaffolds ($R^2 = 0.77$) (Fig. 6B). Increased MSC spread area has also been shown to promote differentiation along the osteogenic lineage[20]; however, there was only a correlation between spread area and ALP activity for 10% G scaffolds ($R^2 = 0.98$, Fig. 6C), suggesting that enhanced cell spreading does not promote differentiation on 5% G scaffolds. The differentiation potential for 5% G scaffolds directly correlates with the percentage of unconfined particles ($R^2 = 0.99$, Fig. 6D), implying that the effective pore size plays a more important role in directing differentiation than the bulk mechanical properties of our scaffolds and the ability of cells to spread on 5% G scaffolds. In addition, on the 10% G–0.1% GTA scaffold where pores were not completely formed (Fig. 2), MSCs were unable to differentiate into osteoblasts (Fig. 5B). Previous work has demonstrated that pore size is critical for bone reformation, which was attributed to enhanced MSC mineralization.[33] Other researchers have postulated that pore size and distribution and surface structure may play an important role in osteogenic differentiation.[33] Our studies demonstrate that the composition of the scaffold can affect whether architectural cues or mechanical cues dominate MSC differentiation.

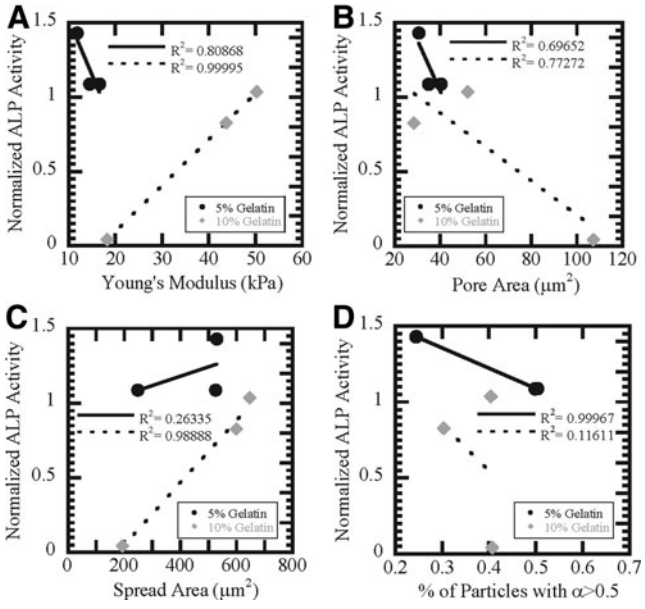

FIG. 6. Correlation of scaffold properties with differentiation potential. Mechanical properties **(A)**, average pore size **(B)**, spread area **(C)**, and the percentage of less-confined particles with $\alpha > 0.5$ **(D)** correlated differently with ALP activity for 5% (black circles) and 10% gelatin (gray diamonds) scaffolds. Linear fits to each data set were performed for 5% (solid line) and 10% (dashed line) scaffolds.

In conclusion, we developed gelatin-GTA scaffolds for the expansion and differentiation of MSCs. The concentration of gelatin and GTA in the scaffold regulated the mechanical and architectural properties, which ultimately determined the differentiation potential of MSCs cultured on the scaffold. These findings may have important implications for scaffold design for tissue engineering applications.

Acknowledgments

The authors would like to acknowledge C. Ononye, D. Ghosh, and C. Kuo for preliminary work on these studies. Funding for this work was provided by the National Science Foundation (1032527) and Emory/Georgia Tech Regenerative Engineering and Medicine Center and the Atlanta Clinical and Translational Science Institute ACTSI. K.M. was supported by the NIH Cell and Tissue Engineering Biotechnology Training Grant (TG GM08433).

Disclosure Statement

No competing financial interests exist.

References

1. Banerjee, I., Mishra, D., and Maiti, T.K. PLGA microspheres incorporated gelatin scaffold: microspheres modulate scaffold properties. Int J Biomater **2009,** 143659, 2009.
2. Lai, J.-Y., Li, Y.-T., Cho, C.-H., and Yu, T.-C. Nanoscale modification of porous gelatin scaffolds with chondroitin sulfate for corneal stromal tissue engineering. Int J Nanomed **7,** 1101, 2012.
3. Huang, Y., Onyeri, S., Siewe, M., Moshfeghian, A., and Madihally, S.V. *In vitro* characterization of chitosan-gelatin scaffolds for tissue engineering. Biomaterials **26,** 7616, 2005.

4. Olde Damink, L.H.H., *et al.* Glutaraldehyde as a cross-linking agent for collagen-based biomaterials. J Mater Sci Mater Med **6,** 460, 1995.
5. Avrameas, S., and Ternynck, T. The cross-linking of proteins with glutaraldehyde and its use for the preaparation of immunoadsorbents. Immunochemistry **6,** 53, 1969.
6. Pittenger, M.F., *et al.* Multilineage potential of adult human mesenchymal stem cells. Science **284,** 143, 1999.
7. Aggarwal, S., and Pittenger, M.F. Human mesenchymal stem cells modulate allogeneic immune cell responses. Blood **105,** 1815, 2005.
8. Bernardo, M.E., *et al.* Human bone marrow–derived mesenchymal stem cells do not undergo transformation after long-term *in vitro* culture and do not exhibit telomere maintenance mechanisms. Cancer Res **67,** 9142, 2007.
9. Kharaziha, P., *et al.* Improvement of liver function in liver cirrhosis patients after autologous mesenchymal stem cell injection: a phase I–II clinical trial. Eur J Gastroenterol Hepatol **21,** 1199, 2009.
10. Falanga, V., *et al.* Autologous bone marrow-derived cultured mesenchymal stem cells delivered in a fibrin spray accelerate healing in murine and human cutaneous wounds. Tissue Eng **13,** 1299, 2007.
11. Horwitz, E.M., *et al.* Isolated allogeneic bone marrow-derived mesenchymal cells engraft and stimulate growth in children with osteogenesis imperfecta: Implications for cell therapy of bone. Proc Natl Acad Sci U S A **99,** 8932, 2002.
12. Lee, R.H., *et al.* Intravenous hMSCs improve myocardial infarction in mice because cells embolized in lung are activated to secrete the anti-inflammatory protein TSG-6. Cell Stem Cell **5,** 54, 2009.
13. Sun, Y., Chen, C.S., and Fu, J. Forcing stem cells to behave: a biophysical perspective of the cellular microenvironment. Annu Rev Biophys **41,** 519, 2012.
14. Silva, E.A., Kim, E.-S., Kong, H.J., and Mooney, D.J. Material-based deployment enhances efficacy of endothelial progenitor cells. Proc Natl Acad Sci U S A **105,** 14347, 2008.
15. Khetan, S., *et al.* Degradation-mediated cellular traction directs stem cell fate in covalently crosslinked three-dimensional hydrogels. Nat Mater **12,** 458, 2013.
16. Mosiewicz, K.A., *et al. In situ* cell manipulation through enzymatic hydrogel photopatterning. Nat Mater **12,** 1072, 2013.
17. Huebsch, N., *et al.* Harnessing traction-mediated manipulation of the cell/matrix interface to control stem-cell fate. Nat Mater **9,** 518, 2010.
18. Kilian, K.A., Bugarija, B., Lahn, B.T., and Mrksich, M. Geometric cues for directing the differentiation of mesenchymal stem cells. Proc Natl Acad Sci U S A **107,** 4872, 2010.
19. Engler, A.J., Sen, S., Sweeney, H.L., and Discher, D.E. Matrix elasticity directs stem cell lineage specification. Cell **126,** 677, 2006.
20. McBeath, R., Pirone, D.M., Nelson, C.M., Bhadriraju, K., and Chen, C.S. Cell shape, cytoskeletal tension, and RhoA regulate stem cell lineage commitment. Dev Cell **6,** 483, 2004.
21. Crocker, J.C., and Grier, D.G. Methods of digital video microscopy for colloidal studies. J Colloid Interface Sci **310,** 298, 1996.
22. McGrail, D.J., Ghosh, D., Quach, N.D., and Dawson, M.R. Differential mechanical response of mesenchymal stem cells and fibroblasts to tumor-secreted soluble factors. PLoS One **7,** e33248, 2012.
23. Ghosh, D., *et al.* Integral role of platelet derived growth factor in mediating transforming growth factor-beta1 dependent mesenchymal stem cell stiffening. Stem Cells Dev **23,** 245, 2014.
24. Peister, A., *et al.* Adult stem cells from bone marrow (MSCs) isolated from different strains of inbred mice vary in surface epitopes, rates of proliferation, and differentiation potential. Blood **103,** 1662, 2004.
25. Untergasser, A., *et al.* Primer3—new capabilities and interfaces. Nucleic Acids Res **40,** e115, 2012.
26. Bigi, A., Cojazzi, G., Panzavolta, S., Rubini, K. and Roveri, N. Mechanical and thermal properties of gelatin films at different degrees of glutaraldehyde crosslinking. Biomaterials **22,** 763, 2001.
27. Valentine, M., *et al.* Investigating the microenvironments of inhomogeneous soft materials with multiple particle tracking. Phys Rev E Stat Nonlin Soft Matter Phys **64,** 061506, 2001.
28. Abete, T., Del Gado, E., and de Arcangelis, L. Gelation kinetics of crosslinked gelatin. Polym Compos **34,** 259, 2013.
29. Brightman, A.O., *et al.* Time-lapse confocal reflection microscopy of collagen fibrillogenesis and extracellular matrix assembly *in vitro*. Biopolymers **54,** 222, 2000.
30. Park, J.S., *et al.* The effect of matrix stiffness on the differentiation of mesenchymal stem cells in response to TGF-β. Biomaterials **32,** 3921, 2011.
31. Choi, Y.S., *et al.* The alignment and fusion assembly of adipose-derived stem cells on mechanically patterned matrices. Biomaterials **33,** 6943, 2012.
32. Pek, Y.S., Wan, A.C.A., and Ying, J.Y. The effect of matrix stiffness on mesenchymal stem cell differentiation in a 3D thixotropic gel. Biomaterials **31,** 385, 2010.
33. Kasten, P., *et al.* Porosity and pore size of beta-tricalcium phosphate scaffold can influence protein production and osteogenic differentiation of human mesenchymal stem cells: an *in vitro* and *in vivo* study. Acta Biomater **4,** 1904, 2008.

Address correspondence to:
Michelle R. Dawson, PhD
School of Chemical and Biomolecular Engineering
Georgia Institute of Technology
311 Ferst Dr., Northwest
Atlanta, GA 30332-0100

E-mail: mdawson@gatech.edu

Received: December 16, 2013
Accepted: May 28, 2014
Online Publication Date: July 7, 2014